Small-World Networks and Their Relationship With Hippocampal Glutamine/Glutamate Concentration in Healthy Adults With Varying Genetic Risk for Alzheimer's Disease

Hui Zhang, PhD,[1,2] Pui W. Chiu, PhD,[1,3] Isaac Ip, PhD,[4] Tianyin Liu, PhD,[5]
Gloria H.Y. Wong, PhD,[5] You-Qiang Song, PhD,[6] Savio W.H. Wong, PhD,[4]
and Karl Herrup, PhD,[7] and Henry K.F. Mak, MD[1,2,3]*

Background: Apolipoprotein E ε4 allele (ApoE4) is the most common gene polymorphism related to Alzheimer's disease (AD). Impaired synaptic dysfunction occurs in ApoE4 carriers before any clinical symptoms. It remains unknown whether ApoE4 status affects the hippocampal neuromodulation, which further influences brain network topology.
Purpose: To study the relationship of regional and global network properties by using graph theory analysis and glutamatergic (Glx) neuromodulation in the ApoE isoforms.
Study Type: Prospective.
Subjects: Eighty-four cognitively normal adults (26 ApoE4 and 58 non-ApoE4 carriers).
Field Strength/Sequence: Gradient-echo echo-planar and point resolved spectroscopy sequence at 3 T.
Assessment: Glx concentration in bilateral hippocampi were processed with jMRUI (4.0), and graph theory metrics (global: γ, λ, small-worldness in whole brain; regional: nodal clustering coefficient (C_i) and nodal characteristic path length (L_i)) in top 20% highly connected hubs of subgroups (low-risk: non-ApoE4; high-risk: APOE4) were calculated and compared.
Statistical Tests: Two-sample t test was used to compare metrics between subgroups. Correlations between regional properties and Glx by Pearson's partial correlation with false discovery rate correction.
Results: Significant differences ($P < 0.05$) in C_i between subgroups were found in hubs of left inferior frontal, bilateral inferior temporal, and bilateral precentral gyri, right parahippocampus, and bilateral precuneus. In addition, there was a significant correlation between Glx in the left hippocampus and C_i in inferior frontal gyrus ($r = -0.537$, $P = 0.024$), right inferior temporal ($r = -0.478$, $P = 0.043$), right parahippocampus ($r = -0.629$, $P = 0.016$), left precentral ($r = -0.581$, $P = 0.022$), right precentral ($r = -0.651$, $P = 0.003$), left precuneus ($r = -0.545$, $P = 0.024$), and right precuneus ($r = -0.567$, $P = 0.022$); and L_i in left precuneus ($r = 0.575$, $P = 0.032$) and right precuneus ($r = 0.586$, $P = 0.032$) in the high-risk group, but not in the low-risk group.
Data Conclusion: Our results suggested that healthy ApoE4 carriers exhibit poorer local interconnectivity. Moreover, the close relationship between glutamate and small-world network properties in ApoE4 carriers might reflect a compensatory response to the impaired network efficiency.
Evidence Level: 2
Technical Efficacy: Stage 3

As the most common form of dementia, Alzheimer's disease (AD) was characterized first by memory loss. The clinical symptoms slowly deteriorate and are accompanied by personality changes, lacking ability to communicate or eat independently and eventually be completely incapable.[1] Since many new treatments are under development to reduce or halt the cognitive decline, there will be an increasing need to identify the individuals likely to develop AD.[2]

The apolipoprotein E ϵ4 allele (ApoE4) is the most important genetic risk factor in the pathogenesis of AD. The age of onset of AD is reduced and the risk of developing AD is increased. Heterozygous and homozygous ϵ4 allele carriers are 3–4 times and 8–12 times, respectively, more likely to develop AD.[3] Thus, a goal for early detection is to investigate the pathogenetic mechanisms in individuals with ApoE4 genotype, who are more likely to develop AD. Bookheimer and Burggren et al provided ample evidence that cognitive impairment in ApoE4 carriers occur before any clinical symptoms.[2] Several neuroimaging studies have demonstrated the ApoE4-mediated modulation of cortical thickness,[4] intrinsic functional brain networks,[5] and glucose hypometabolism[6] in cognitively normal subjects. Also, Chen et al's study showed that ApoE4 isoform reduces the glutamate function and synaptic plasticity.[7] These results proved that the abnormal physiological and metabolic changes occurred before the confirmed pathology.

Advances in neuroscience have improved our knowledge of the human brain, which has been proven to operate as a complex network. Graph theory analysis of the human brain provides a quantitative way to measure the neural interconnections among synapses and axonal pathways which could assist in exploring or demonstrating anatomical development or pathological changes.[8] Studies have demonstrated that the human brain possess "small world" properties, i.e. higher local clustering coefficients and preserved path length compared to matched random networks, which maintain a balance between local segregation (local clustering) and global integration (path length) to optimize the information processing efficiency.[8,9] Based on different neuroimaging techniques (functional, diffusion magnetic resonance imaging [MRI], and ^{18}F-fluorodeoxyglucose positron emission tomography [FDG-PET]), the human brain networks demonstrated disrupted topological configurations in disease.[2] Intriguingly, impaired function of the networks and topological configurations of the brain have been reported in the ApoE4 carriers of cognitively normal individuals.[10–12] ApoE4 carriers showed an accelerated age-related loss of local interconnectivity (clustering coefficient).[10] Using FDG-PET, Seo et al[12] found lower local clustering and path length in cognitively normal elderly carriers compared to noncarriers. However, it remains largely unknown how ApoE4 allele modulates the dynamic balance between segregation and integration in the brain.

Shine's study suggested two neuromodulatory systems (noradrenergic and cholinergic systems) have a strong influence over the dynamic cortical balance.[13] Research related to memory loss and dementia has shown impaired cholinergic transmission in the septo-hippocampal pathway.[14] Also, mounting evidence indicated that AD begins with subtle changes in synaptic function from entorhinal cortex and hippocampus.[1,7,15] To our knowledge, there is no study evaluating glutamatergic concentration changes in hippocampal regions by magnetic resonance spectroscopy (MRS) and the topological organization of brain networks (by functional MRI [fMRI]) in the pathogenesis of ApoE4 isoforms. Such an investigation will advance our understanding of the genetic effects in AD on synaptic function.

In this study, resting-state fMRI (rs-fMRI) and graph theory technique were applied to assess and compare the local segregation and global integration between cognitively normal low-risk (non-ApoE4 carriers) and high-risk (ApoE4 carriers) subjects. Then we further evaluated the relationships between those topological properties and glutamate concentrations in bilateral hippocampi to achieve a better understanding of the neuromodulatory mechanism. We hypothesized that the ApoE4 allele affects the dynamic balance between segregation and integration in the brain through synaptic neuromodulation.

Materials and Methods

Subjects

Ethical approval of the research protocol was obtained from the Institutional Review Board of the University and the Hospital Authority, and the study complied with the Declaration of Helsinki. Written informed consent was obtained from all subjects.

Subjects aged 20–60 years were recruited by advertisement on the university campus recreation and sports service centers. Ambulatory community-living older adults (aged 60–80 years) were recruited from social centers for the elderly.

Inclusion criteria included right-handedness, normal blood pressure (less than 140/90 mmHg), and a Montreal Cognitive Assessment (MoCA) cognitive score ≥26. The exclusion criteria included the following: color-blindness; history of stroke, head injury, seizures, migraine, or cancer within 5 years; active infection; end-stage renal or other organ failure; nonambulatory, psychiatric diseases; regular alcohol consumption; and drug abuse.

Participants were interviewed to gather socio-demographic data (age, sex, and educational years), self-reported smoking and alcohol history, drug or substance abuse, history of memory impairment and cognitive complaints, past medical history, and related medications. After the interview, all the subjects underwent the blood pressure measurement and MoCA[16] on the same day before the MRI examination by a trained research associate.

Genotyping

Blood samples were collected immediately after examinations. The samples were frozen and sent to the university for ApoE genotype

analysis using a polymerase chain reaction based method. The ApoE ε alleles of each subject were determined as described by Calero et al.[17] As ApoE has three common allelic forms (ApoE 2, 3, and 4), participants were divided into groups based on the presence or absence of the ApoE4 allele: low-risk group (ApoE 2/2, ApoE 2/3, ApoE 3/3) and high-risk group (ApoE 2/4, ApoE 3/4, ApoE 4/4).

Acquisition of MRI Data

All structural MRI, MRS, and functional data were acquired on a Philips-3T (Achieva) MR scanner using a standard eight-channel head coil (Fig. 2a,b).

Structural images were acquired with a three-dimensional (3D) T1-weighted fast field echo sequence in the sagittal orientation with the repetition time (TR) = 7 msec, the echo time (TE) = 3.2 msec, flip angle = 8°, voxel size = $1 \times 1 \times 1$ mm^3, and FOV = $240 \times 240 \times 160$ (mm).

Single voxel spectroscopy was performed with the following parameters: TR/TE = 2,000/39 msec, number of signals averaged = 128, phase cycles = 16, spectral width = 2,000 Hz with spectral resolution of 1.95 Hz per point, and free induction decay = 1024. Point resolved spectroscopy was used as the volume selection method for the region of interest and the excitation method for water suppression. For shimming, pencil-beam was employed. A $2.5 \times 1.5 \times 1$ cm^3 voxel was placed in both the left and right hippocampi (LH and RH; Fig. 1).

The resting state functional images were collected with a gradient-echo echo-planar sequence in axial orientation sensitive to blood-oxygen-level-dependent contrast: TR = 2000 msec, TE = 30 msec, flip angle = 90°, voxel size = $3.6 \times 3.6 \times 4$ mm^3, FOV = $230 \times 230 \times 128$ (mm), and 32 slices. During the functional scanning, participants were instructed to focus on a cross in the mirror and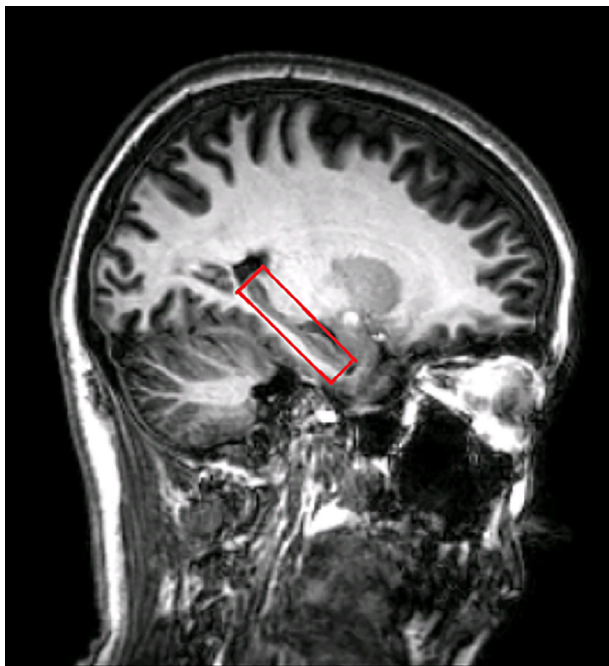 not to think of anything in particular. The rs-fMRI data included 240 functional dynamics lasting for 8 minutes and 16 seconds.

MRS Data Analysis

The combination of glutamate and glutamine concentrations (Glx) processing was conducted using protocols described in detail previously[18–20] (Fig. 2b). Briefly, MRS spectra were processed with jMRUI (4.0) software. One file was the actual (suppressed) MRS data, and the other file was the unsuppressed water signal intensity MRS file. The unsuppressed water signal was measured and used as an internal reference to calculate the absolute concentration of the metabolite under investigation.[21] Spectrum simulation of various metabolites was completed using the built-in NMR-SCOPE. Signal amplitudes were determined using QUEST (quantification based on quantum estimation).[22] Only metabolite estimates with Cramer Rao lower bounds <20% were used for statistical analysis. In summary, absolute concentrations of Glx with cerebrospinal fluid (CSF) correction ($[Glx]_{abs\_CSFcorr.}$) was measured and quantified using internal water as reference by QUEST in jMRUI (4.0). In order to account for the variations in water content in grey matter (GM), white matter (WM), and CSF, voxel-based morphometry was used to determine the GM, WM, and CSF composition within the voxel of each of the two hippocampal regions investigated, as detailed in our previous publications.[18]

Rs-fMRI Data Analysis

IMAGE PREPROCESSING AND NETWORK CONSTRUCTION.
Preprocessing of the rs-fMRI data was performed using the DPABI toolbox (http://rfmri.org/) based on SPM12 (https://www.fil.ion.ucl.ac.uk/spm/software/spm12/) (Fig. 2c). The first 10 dynamics were discarded, and the differences in image acquisition time of the remaining fMRI images were corrected. Next, the time series of images for each subject were realigned using a six-parameter (rigid body) linear transformation with a two-pass procedure (registered to the first image and then registered to the mean of the images after the first realignment). Subjects with head movements more than 3 mm in any direction of x, y, and z or over 3° were excluded in the further analysis. The segmentation procedure was performed on the structural images to generate the tissue maps. In addition, the Diffeomorphic Anatomical Registration Through Exponentiated Lie algebra (DARTEL) tool[23] normalized the structural images and tissue maps to Montreal Neurological Institute (MNI) space and created transformation parameters. Several nuisance signals, including Friston 24 head motion parameters[24] derived from realignment and mean WM and CSF time series within WM and CSF brain masks created from segmentation, were regressed out from the time course in each voxel. All the fMRI images were spatially normalized to the MNI space and resampled to $3 \times 3 \times 3$ mm^3 using the transformation parameters that were estimated through DARTEL segmentation. After the normalization, the data were band-pass filtered ($0.01 < f < 0.08$ Hz) to reduce high-frequency respiratory and cardiac noise and low-frequency drift. Linear trends were also removed.

Based on the automated anatomical labeling template,[25] the preprocessed fMRI data were segmented into 90 regions (45 regions per hemisphere). For each individual, the regional time series was obtained by averaging the time series over all voxels of the region.
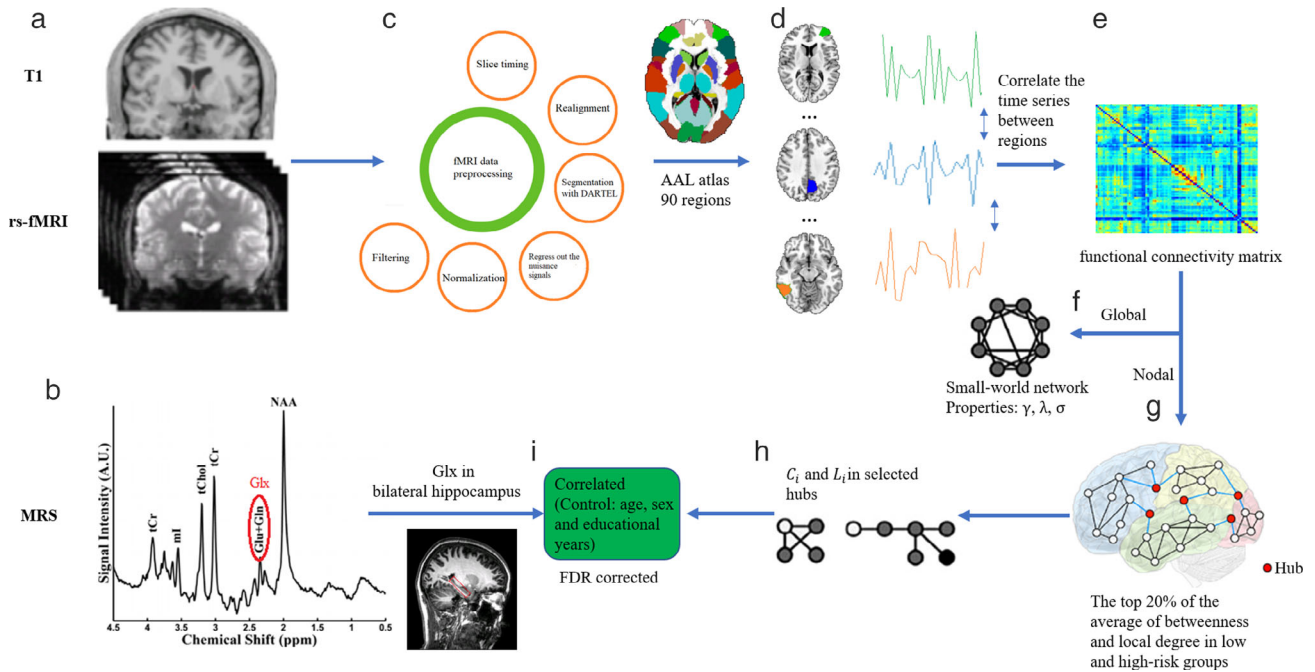

FIGURE 1: Position of magnetic resonance spectroscopy voxel (red box) placed in the left and right hippocampi.

FIGURE 2: Schematic representation of analysis workflow: For each subject, the raw data including **(a)** structural, functional magnetic resonance (MR) images and **(b)** MR spectroscopy data were acquired using MR scanner. Glx concentration in bilateral hippocampus were processed with jMRUI (4.0) with unsuppressed water signal used as an internal reference. **(c)** After preprocessing of the rs-fMRI data, we used the automated anatomical labeling atlas and this parcellation divided the cortical surface into 90 regions. **(d)** Several time series were extracted from each region. **(e)** After retrieval of the mean individual regional time series, we calculated the correlation coefficients between the pairs and formed a standard 90 × 90 FC matrix for each person. All the topological metrics in **(f)** global and **(g)** nodal level were estimated using small world network analysis. The top 20% of the sum of the ranking scores based on the local betweenness centrality and local degree were selected as the network hubs. **(h)** Referring to the hubs with significant differences between low and high-risk groups, **(i)** the relationship between topological measurements (C_i and L_i of hubs) and $[Glx]_{abs\_CSFcorr.}$ in left and right hippocampal regions was estimated controlling for the effect of age, sex, and educational years using the Pearson's partial correlation method with false discovery rate correction.

After retrieval of the mean individual regional time series, we calculated the correlation coefficients between the pairs and formed a standard 90 × 90 functional connectivity (FC) matrix for each person (Fig. 2d,e). The Fisher Z-transformation was applied to transform the correlation coefficients so that the data was normally distributed.

TOPOLOGICAL PROPERTIES OF WEIGHTED BRAIN NETWORKS.
Graph theoretical analyses were performed on the 90 × 90 FC matrix for each subject using the Graphvar toolbox.[26] Instead of selecting a single threshold, we investigated the topological properties over a range of threshold levels. For a given network G, the definition of connection density is the number of edges in G to the maximal possible edge number. In the analysis, the cost of the network below 37% would start to fragment, and more than 50% the network becomes more random. To interpret the topological properties, we applied a wide range of connection densities from 37% to 50%.[27] All the topological metrics in global (Fig. 2f) and nodal level (Fig. 2g) were estimated using the averages of measures taken from each subject's network in the range of network cost 37–50% with an interval of 1%.

Two measures were employed to measure the topological properties of local brain regions: the nodal clustering coefficient (C_i) and the nodal characteristic path length (L_i).[28] The nodal clustering coefficient is a measurement of function segregation in the brain,

which is the ability for specialized information processing within widely interconnected groups of the brain network and measures the cliquishness of the node's neighborhood.[9] The characteristic path length of a node is a basic measure of brain functional integration which is a capability to rapidly integrate information from distributed regions.

The global network architecture of functional network was characterized by three parameters: the normalized clustering coefficient (γ), the normalized characteristic path length (λ), and the small-worldness (σ).[28] The global clustering coefficient and the global characteristic path length, C and L, is the average of the nodal clustering coefficients (C_i) and the nodal characteristic path length (L_i) of all nodes in the network. C and L are often normalized to 100 matched random networks with the same numbers of nodes, edges, and degree distribution as the real networks. The normalized clustering coefficient $\gamma = C/C^{rand}$ and the normalized characteristic path length $\lambda = L/L^{rand}$ were computed to examine the small-worldness of the network. C^{rand} and L^{rand} represent the means of the corresponding metrics derived from those matched random networks. As a small-world network, it should meet the standard $\gamma > 1$ and $\lambda \approx 1$ or the small-worldness $\sigma = \gamma/\lambda > 1$.[9]

SELECTION OF HUBS.
Based on Xu et al,[29] the local betweenness centrality and local degree were combined together to select hubs of a network, where a hub is identified as a region with high

degree of connectivity to other parts of the brain. The values of the two indexes were averaged in the two hemispheres and ranked in descending order respectively in low-risk and high-risk groups. The top 20% of the sum of the ranking scores were selected as the network hubs (Fig. 2g). The nodal clustering coefficient (C_i) and the nodal characteristic path length (L_i) in those selected hubs were calculated and correlated with the Glx concentrations in bilateral hippocampus (Fig. 2h,i).

Statistical Analysis

Statistical analysis was performed using SPSS (SPSS, Inc., Chicago, IL, USA). Sex difference between the groups was tested using Pearson's chi-square test. Two-sample t tests were applied to investigate group differences in demographic results and graph metrics (local metrics for each hub and global metrics for whole brain).

Referring to the regions with significant differences in two sample t-test results, the relationship between topological measurements (C_i and L_i of hubs) and [Glx]$_{abs\_CSFcorr.}$ in left and right hippocampal regions was estimated controlling for the effect of age, sex, and educational years using the Pearson's partial correlation method. The scatter plots showing the relationships between topological properties (C_i and L_i of hubs) and [Glx]$_{abs\_CSFcorr.}$ in left and right hippocampal regions were created. A significance level was set at $P < 0.05$ for all statistical tests, and the correlation analyses were performed with corrections for multiple comparisons by using false discovery rate (FDR) correction.

Results

Ninety-one healthy, cognitively normal subjects (age: range from 20 to 84 years old, mean ± standard deviation: 51 ± 16.6 years old, sex: 58 female/33 male) were enrolled. Seven subjects were excluded because of head motion in the rs-fMRI. In addition, there are four subjects with head motion in MRS session. Finally, 84 subjects were available for network analysis and 80 subjects for the correlation between MRS parameters and network properties.

The top 20% of brain regions regarded as network hubs are shown in Table 1. Table 2 shows the demographic information, neuropsychological test results, [Glx]$_{abs\_CSFcorr.}$ and global small-world network properties of the low- and high-risk groups.

The small worldness (σ) of FC brain networks in two groups were: γ/λ for the ApoE4 carriers: 1.23 ± 0.10/1.12 ± 0.05; for non-ApoE4 carriers: 1.20 ± 0.11/1.11 ± 0.07. There was no significant difference between these two groups in sex ($P = 0.08$), age range ($P = 0.31$), educational years ($P = 0.36$), MoCA score ($P = 0.91$), [Glx]$_{abs\_CSFcorr.}$ in the left ($P = 0.50$) and right ($P = 0.92$) hippocampus, or global graph metrics γ ($P = 0.23$), λ ($P = 0.33$), and σ ($P = 0.38$).

The resulting graph metrics (clustering coefficient C_i and characteristic path length L_i) of low- and high-risk groups for each hub is displayed in Fig. 3. The clustering coefficients of hubs in the ε4 allele noncarriers were significantly higher

than the high-risk carriers, and especially in left inferior frontal gyrus, bilateral inferior temporal gyrus, right parahippocampus, bilateral precentral gyrus, and bilateral precuneus. Meanwhile, longer regional characteristic path lengths were found in the high-risk group, but it was not significantly different in the group comparison.

There was a significant relationship between [Glx]$_{abs\_CSFcorr.}$ in left hippocampus and topological metrics (C_i and L_i, $P < 0.05$, FDR-corrected) in high-risk but not low-risk group: Significant correlation was found between [Glx]$_{abs\_CSFcorr.}$ in LH and C_i in orbital part of left inferior frontal gyrus ($r = -0.537$, $P = 0.024$), right inferior temporal gyrus ($r = -0.478$, $P = 0.043$), right parahippocampus ($r = -0.629$, $P = 0.016$), left precentral gyrus ($r = -0.581$, $P = 0.022$), right precentral gyrus ($r = -0.651$, $P = 0.003$), left precuneus ($r = -0.545$, $P = 0.024$), and right precuneus ($r = -0.567$, $P = 0.022$) (Table 3 and Fig. 4). Also, L_i in left precuneus ($r = 0.575$, $P = 0.032$) and right precuneus ($r = 0.586$, $P = 0.032$) showed statistical correlation with [Glx]$_{abs\_CSFcorr.}$ in left hippocampus (Table 4 and Fig. 4).

Discussion

In this study, significant decreases were found in cluster coefficients in a number of regions in the high-risk group, including the left inferior frontal gyrus, bilateral inferior temporal gyrus, right parahippocampus, bilateral precentral gyrus, and bilateral precuneus. No significant difference was detected in the characteristic path length. In a nutshell, there was a significant difference in local segregation (clustering coefficient), but not in global functional integration (characteristic path length) when comparing the two groups.

The small-world organization reflects the balance of local segregation and global integration in a real network compared to a random network.[10] Although no significant difference of small-world network was revealed in the group comparison, our findings indicated loss of local segregation exceed global integration.

As a measure of the local interconnectivity of the complex real network, the clustering coefficient reflects the clustering edges which had higher value in being connected tightly with their neighborhood. The lower clustering coefficients in inferior frontal gyrus, precuneus/posterior cingulate cortex (PCC), inferior temporal, precentral, and para-hippocampus in the high-risk group represented disrupted connections with their neighborhoods, suggesting that the economic arrangement of these brain networks was likely impaired in ApoE4 carriers. The short-range connections were interrupted which might lead to worse fault tolerance in the information transfer process and slower modularized information-processing speed.[29]

The existence of hubs is essential to maintain network-wide information flow and most of those hubs correspond to

TABLE 1. Hubs Identified From Subgroups

Regions	Abbreviation	Low-Risk Group	High-Risk Group
Anterior cingulate and paracingulate gyri (left)	ACC.L	✓	✓
Inferior frontal gyrus, orbital part (left)	IFGorb_L		✓
Inferior frontal gyrus, orbital part (right)	IFGorb_R		✓
Inferior temporal gyrus (left)	ITG_L	✓	
Inferior temporal gyrus (right)	ITG_R	✓	✓
Median cingulate and paracingulate gyri (left)	MCC_L	✓	✓
Median cingulate and paracingulate gyri (right)	MCC_R	✓	✓
Middle frontal gyrus (left)	MFG_L	✓	✓
Middle frontal gyrus (right)	MFG_R	✓	✓
Middle temporal gyrus (left)	MTG_L	✓	✓
Middle temporal gyrus (right)	MTG_R	✓	✓
Parahippocampus (right)	PHIP_R	✓	
Precentral gyrus (left)	PreCG_L	✓	✓
Precentral gyrus (right)	PreCG_R	✓	✓
Precuneus (left)	PCNU_L	✓	✓
Precuneus (right)	PCNU_R		✓
Superior frontal gyrus, dorsolateral (right)	SFGdor_R	✓	✓
Superior temporal gyrus (left)	STG_L	✓	
Superior temporal gyrus (right)	STG_R	✓	✓
Temporal pole: superior temporal gyrus (left)	STGp_L	✓	✓
Temporal pole: superior temporal gyrus (right)	STGp_R	✓	✓

✓ indicates a hub.

high metabolic activity.[8] Hubs like the left inferior frontal gyrus, right inferior temporal gyrus, right parahippocampus, bilateral precentral gyrus, and bilateral precuneus showed significant differences between the two groups. These results were consistent with previous findings.[5,30–34] Precuneus/PCC is particularly vulnerable at the preclinical stage before AD onset.[30] As a "seed" region of interest in deriving the spatial pattern of the default mode network (DMN), the precuneus/PCC in ApoE4 carriers exhibited abnormalities in prior studies, including reduced cortical thickness[30,32] and impaired functional connectivity with several regions in the DMN or other networks.[32] Previous fMRI findings also suggested a central role for the precuneus/PCC in episodic memory,[31,33] and regions like left ventro-lateral frontal region/frontal operculum,[33] right parahippocampus,[5] and inferior temporal gyrus[34] were also involved. Memory decline occurred earlier in cognitively healthy ApoE4 carriers than noncarriers and preceded clinically detectable AD.[35] Interestingly, network impairment occurred in bilateral precentral gyri of high-risk groups. This result might provide evidence that the sensorimotor cortex has functional changes before any pathological symptoms.

Another major finding in this study is the significant negative correlation between the major neurotransmitter glutamate in LH and clustering coefficients of several hubs and significant positive correlation between glutamate in LH and characteristic path length of bilateral precuneus in the ApoE4 carriers.

We speculate that glutamate might modulate the brain network function, especially the function in the hubs from cognitive-related (memory) networks. Chen et al[7] discovered that the ApoE4 isoform selectively impaired synaptic plasticity and the phosphorylation of N-methyl-D-aspartate is the expansion (NMDA) receptor by a regular called Reelin. In an animal study, ApoE4 was found to stimulate the accumulation of tau and Aβ42 and decrease the VGlut concentration

TABLE 2. Demographic Information, Neuropsychological Test Results, [Glx]$_{abs\_CSFcorr.}$ and Global Graph Metrics of Low- and High-Risk Groups

	Low-Risk Group (Non-ApoE4 carrier)	High-Risk Group (ApoE4 carrier)	*P*-Value
Number (*N*)	58	26	–
Sex (female/male)	33 F/25 M	20 F/6 M	0.08
Age range	49.35 ± 16.74	53.35 ± 15.67	0.31
Educational years	14.77 ± 4.48	13.81 ± 4.17	0.36
MoCA	28.88 ± 1.26	28.85 ± 1.12	0.91
[Glx]$_{abs\_CSFcorr.}$ in left hippo	14.18 ± 3.25 (*N* = 57)	13.62 ± 3.52 (*N* = 23)	0.50
[Glx]$_{abs\_CSFcorr.}$ in right hippo	13.77 ± 3.44 (*N* = 57)	13.86 ± 3.48 (*N* = 23)	0.92
γ	1.20 ± 0.11	1.23 ± 0.10	0.23
λ	1.11 ± 0.07	1.12 ± 0.05	0.33
σ	1.08 ± 0.06	1.10 ± 0.05	0.38

"–"indicates not applicable. Unless otherwise noted, values are presented as mean ± standard deviation. γ is the normalized global clustering coefficient, λ is the normalized global characterisitic path length, and σ is the small worldness.
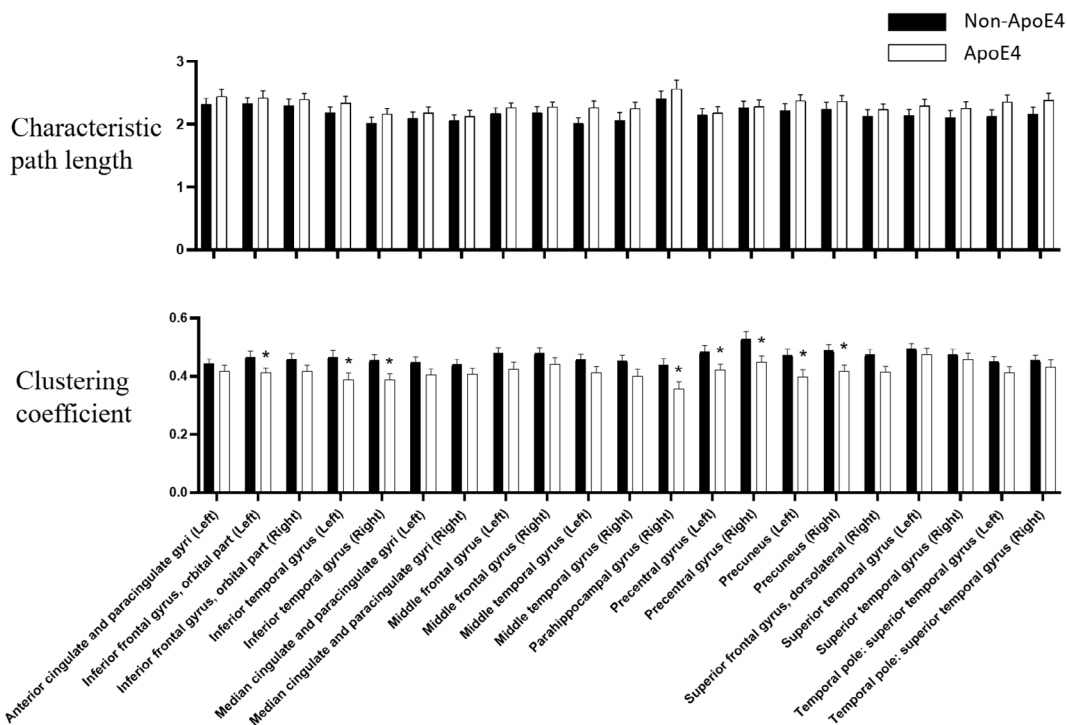

FIGURE 3: Bar plots of the clustering coefficients (C_i) and characteristic path lengths (L_i) for each region for ApoE4 and non-ApoE4 carriers (* indicates $P < 0.05$).

in hippocampal gyrus which was related to the cognition decline.[15] We postulate that due to ApoE4-induced neural connectivity impairment, increased efficiency of the production of neurochemicals within left hippocampal glutamatergic pathways was required.

Previous studies have mentioned mechanisms of neuromodulation,[13,36] such as fast (ionotropic-mediated) and slow (metabotropic-mediated) mechanisms. Numerous modulatory nuclei include neurons which can project the neurotransmitters glutamate and gamma-aminobutyric acid (GABA)

TABLE 3. Relationship Between $[Glx]_{abs\_CSFcorr.}$ and Clustering Coefficient C_i in Low- and High-Risk Groups, Controlling for Age, Sex, and Educational Years

Regions Clustering coefficient	Low Risk (N = 57)				High Risk (N = 23)			
	Glx_LH		Glx_RH		Glx_LH		Glx_RH	
	r	P	r	P	r	P	r	P
Inferior frontal gyrus, orbital part (left)	−0.076	0.979	0.017	0.977	−0.537	0.024*	−0.258	0.569
Inferior temporal gyrus (left)	−0.081	0.979	−0.073	0.977	−0.025	0.919	−0.505	0.224
Inferior temporal gyrus (right)	−0.005	0.979	−0.070	0.977	−0.478	0.043*	0.055	0.824
Parahippocampus (right)	−0.055	0.979	0.004	0.977	−0.629	0.016*	0.066	0.824
Precentral gyrus (left)	0.012	0.979	−0.078	0.977	−0.581	0.022*	0.214	0.569
Precentral gyrus (Right)	−0.037	0.979	−0.091	0.977	−0.651	0.016*	0.194	0.569
Precuneus (left)	0.021	0.979	0.028	0.977	−0.545	0.024*	0.232	0.569
Precuneus (right)	0.004	0.979	0.021	0.977	−0.567	0.022*	0.236	0.569

*$P < 0.05$, and the P-values were adjusted with false discovery rate correction method.
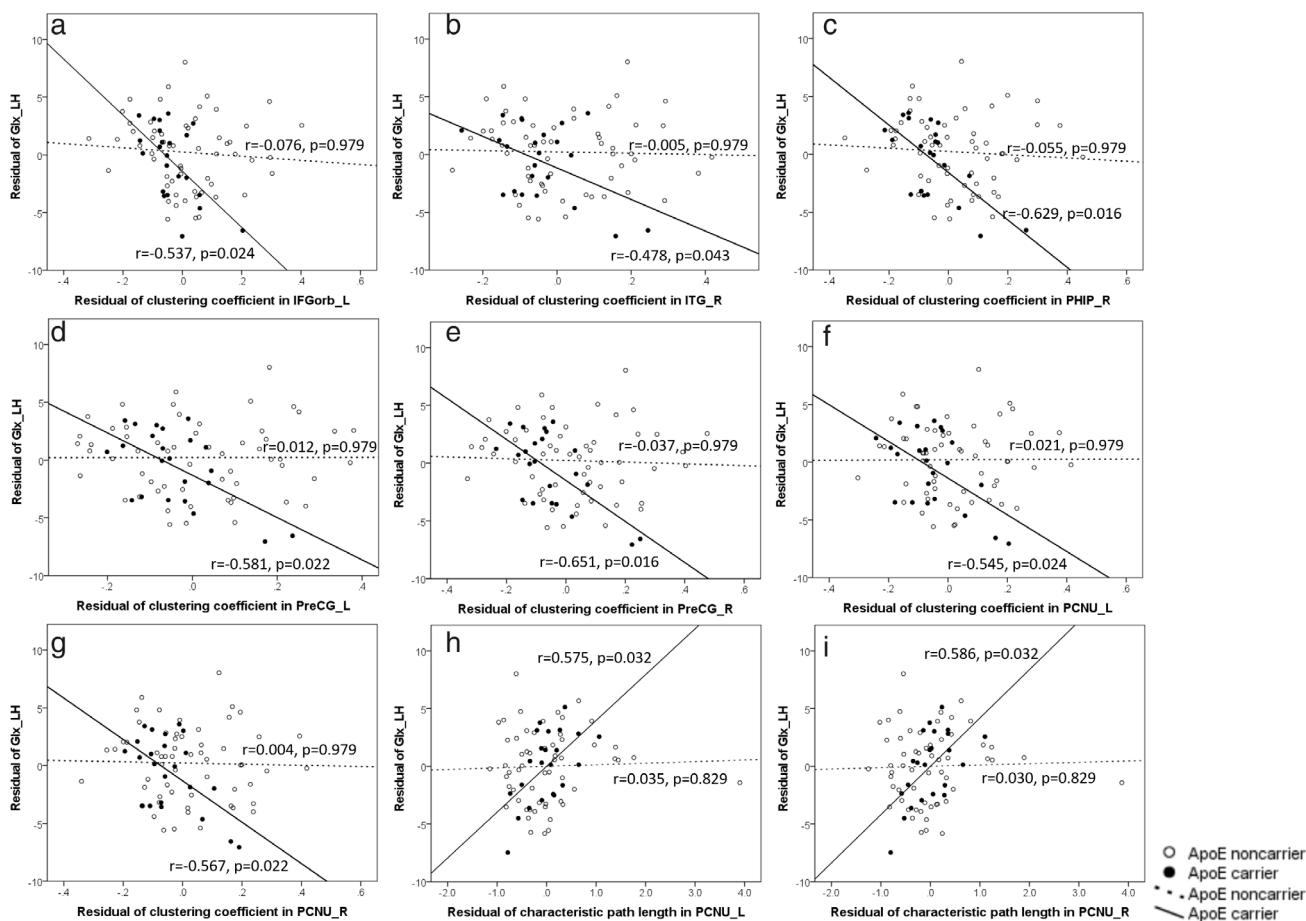

FIGURE 4: Scatter plots showing partial correlations controlled for age, sex, and educational years between the $[Glx]_{abs\_CSFcorr.}$ in left hippocampus and clustering coefficients in the (a) left orbital part in inferior frontal gyrus (IFGorb_L), (b) right inferior temporal gyrus (ITG_R), (c) right parahippocampus (PHIP_R), (d) left precentral gyrus (PreCG_L), (e) right precentral gyrus (PreCG_R), (f) left precuneus (PCNU_L), and (g) right precuneus (PCNU_R); and between the $[Glx]_{abs\_CSFcorr.}$ in left hippocampus and characteristic path length in the (h) left precuneus (PCNU_L) and (i) right precuneus (PCNU_R).

TABLE 4. Relationship Between [Glx]$_{abs\_CSFcorr.}$ and Characteristic Path Length L_i in the Low- and High-Risk Groups, Controlling for Age, Sex, and Educational Years

| Regions Characteristic path length | Low Risk (N = 57) | | | | High Risk (N = 23) | | | |
| | Glx_LH | | Glx_RH | | Glx_LH | | Glx_RH | |
	r	P	r	P	r	P	r	P
Inferior frontal gyrus, orbital part (left)	0.098	0.683	−0.015	0.950	0.383	0.095	0.135	0.706
Inferior temporal gyrus (left)	0.091	0.683	0.033	0.950	0.483	0.083	−0.322	0.370
Inferior temporal gyrus (right)	0.097	0.683	−0.013	0.950	0.456	0.086	−0.309	0.370
Parahippocampus (right)	0.128	0.683	−0.009	0.950	0.419	0.086	−0.072	0.762
Precentral gyrus (left)	0.105	0.683	0.080	0.950	0.409	0.086	−0.119	0.706
Precentral gyrus (right)	0.127	0.683	0.102	0.950	0.407	0.086	−0.145	0.706
Precuneus (left)	0.035	0.829	−0.014	0.950	0.575	0.032*	−0.391	0.370
Precuneus (right)	0.030	0.829	−0.018	0.950	0.586	0.032*	−0.340	0.370

*$P < 0.05$, and the P-values were adjusted with false discovery rate correction method.

with slow neurochemical changes, and this will sustain the capability to act on the signals in a faster and more targeted fashion (more or less likely to fire). Shine's study shed light on the neurochemical modulatory mechanisms on the brain networks i.e. the cholinergic system promotes relatively segregated network topology and noradrenergic locus coeruleus facilitates integration.[13] In our study, there were more significantly correlated regions in local segregation (seven out of eight) in comparison with global integration (two out of eight). We proposed that the neuromodulation in the cholinergic and noradrenergic systems of the ApoE4 and non-ApoE4 carriers could act different from the usual manner. The neuromodulatory influences on both segregation by cholinergic system and integration by noradrenergic system might be impaired in ApoE4 group. To compensate for the weakened modulation by these two systems, the glutamatergic system might exert its effect mostly on the brain network segregation, albeit to a much lesser extent on the integration.

Furthermore, significant modulation was only found in the [Glx]$_{abs\_CSFcorr.}$ in left side of hippocampus. Previous studies mentioned the left–right asymmetry of hippocampal synapses.[37,38] In our study, the cause of the asymmetrical correlation was unknown. As a possible mechanism in the developmental perspective, we hypothesized the role of ApoE4 as an example of antagonistic pleiotropy.[39]

Limitations

First, the drawback of steady state MRS technique was the unknown composition of synaptic and intracellular glutamate and glutamine. We would like to emphasize that as the purpose of our study was to evaluate the glutamatergic system of healthy adults (with tight coupling of glutamate and glutamine),[40] it was justified to measure Glx (glutamate plus glutamine), instead of analyzing glutamate and glutamine separately. Second, our study measured values at a single time point. Longitudinal studies will be necessary to study the time course of any alterations in resting state functional connectivity and to determine the optimal timing for potential interventional studies in individuals at risk for AD. Third, our study had a relatively small sample size with unequal number of participants in each group.

Conclusion

Our results suggest that ApoE4 carriers exhibit poorer local interconnectivity compared to noncarriers. The close relationship we observed between glutamate and topological properties in ApoE4 carriers might reflect the compensation for impaired cortical communication efficiency. Combined MRS and resting-state fMRI may assist in preclinical assessment of AD, especially of the high-risk carriers.

Acknowledgments

REFERENCES

1. Braak H, Braak E, Bohl J. Staging of Alzheimer-related cortical destruction. Eur Neurol 1993;33(6):403-408.

2. Bookheimer S, Burggren A. APOE-4 genotype and neurophysiological vulnerability to Alzheimer's and cognitive aging. Annu Rev Clin Psychol 2009;5:343-362.

3. Heffernan AL, Chidgey C, Peng P, Masters CL, Roberts BR. The neurobiology and age-related prevalence of the epsilon4 allele of apolipoprotein E in Alzheimer's disease cohorts. J Mol Neurosci 2016;60(3): 316-324.

4. Burggren AC, Zeineh M, Ekstrom AD, et al. Reduced cortical thickness in hippocampal subregions among cognitively normal apolipoprotein E e4 carriers. Neuroimage 2008;41(4):1177-1183.

5. Chen Y, Chen K, Zhang J, et al. Disrupted functional and structural networks in cognitively normal elderly subjects with the APOE varepsilon4 allele. Neuropsychopharmacology 2015;40(5):1181-1191.

6. Reiman EM, Chen K, Alexander GE, et al. Correlations between apolipoprotein E ε4 gene dose and brain-imaging measurements of regional hypometabolism. Proc Natl Acad Sci 2005;102(23):8299-8302.

7. Chen Y, Durakoglugil MS, Xian X, Herz J. ApoE4 reduces glutamate receptor function and synaptic plasticity by selectively impairing ApoE receptor recycling. Proc Natl Acad Sci U S A 2010;107(26):12011-12016.

8. Farahani FV, Karwowski W, Lighthall NR. Application of graph theory for identifying connectivity patterns in human brain networks: A systematic review. Front Neurosci 2019;13:585.

9. Watts DJ, Strogatz SH. Collective dynamics of "small-world" networks. Nature 1998;393(6684):440-442.

10. Brown JA, Terashima KH, Burggren AC, et al. Brain network local interconnectivity loss in aging APOE-4 allele carriers. Proc Natl Acad Sci U S A 2011;108(51):20760-20765.

11. Foo H, Mather KA, Jiang J, Thalamuthu A, Wen W, Sachdev PS. Genetic influence on ageing-related changes in resting-state brain functional networks in healthy adults: A systematic review. Neurosci Biobehav Rev 2020;113:98-110.

12. Seo EH, Lee DY, Lee JM, et al. Influence of APOE genotype on whole-brain functional networks in cognitively normal elderly. PLoS One 2013;8(12):e83205.

13. Shine JM. Neuromodulatory influences on integration and segregation in the brain. Trends Cogn Sci 2019;23(7):572-583.

14. Khakpai F, Nasehi M, Haeri-Rohani A, Eidi A, Zarrindast MR. Septo-hippocampo-septal loop and memory formation. Basic Clin Neurosc 2013;4(1):5.

15. Liraz O, Boehm-Cagan A, Michaelson DM. ApoE4 induces Abeta42, tau, and neuronal pathology in the hippocampus of young targeted replacement apoE4 mice. Mol Neurodegener 2013;8:16.

16. Wong A, Xiong YY, Kwan PW, et al. The validity, reliability and clinical utility of the Hong Kong Montreal cognitive assessment (HK-MoCA) in patients with cerebral small vessel disease. Dement Geriatr Cogn Disord 2009;28(1):81-87.

17. Calero O, Hortiguela R, Bullido MJ, Calero M. Apolipoprotein E genotyping method by real time PCR, a fast and cost-effective alternative to the TaqMan and FRET assays. J Neurosci Methods 2009;183(2): 238-240.

18. Chiu PW, Lui SSY, Hung KSY, et al. In vivo gamma-aminobutyric acid and glutamate levels in people with first-episode schizophrenia: A proton magnetic resonance spectroscopy study. Schizophr Res 2018;193: 295-303.

19. Chiu PW, Mak HK, Chan Y, Chan T, Ho KM. Hippocampal MR spectroscopic abnormalities in a cohort of syphilitic patients with HIV and neurosyphilis infection. Am J Nucl Med Mol Imaging 2015;5(1):83-94.

20. Chiu PW, Mak HK, Yau KK, Chan Q, Chang RC, Chu LW. Metabolic changes in the anterior and posterior cingulate cortices of the normal aging brain: Proton magnetic resonance spectroscopy study at 3 T. Age (Dordr) 2014;36(1):251-264.

21. de Graaf RA. In vivo NMR spectroscopy: Principles and techniques. 2nd ed. Chichester: Wiley; 2007.

22. Seeger U, Klose U, Mader I, Grodd W, Nagele T. Parameterized evaluation of macromolecules and lipids in proton MR spectroscopy of brain diseases. Magn Reson Med 2003;49(1):19-28.

23. Ashburner J. A fast diffeomorphic image registration algorithm. Neuroimage 2007;38(1):95-113.

24. Friston KJ, Williams S, Howard R, Frackowiak RS, Turner R. Movement-related effects in fMRI time-series. Magn Reson Med 1996;35(3): 346-355.

25. Tzourio-Mazoyer N, Landeau B, Papathanassiou D, et al. Automated anatomical labeling of activations in SPM using a macroscopic anatomical parcellation of the MNI MRI single-subject brain. Neuroimage 2002; 15(1):273-289.

26. Kruschwitz JD, List D, Waller L, Rubinov M, Walter H. GraphVar: A user-friendly toolbox for comprehensive graph analyses of functional brain connectivity. J Neurosci Methods 2015;245:107-115.

27. Lynall ME, Bassett DS, Kerwin R, et al. Functional connectivity and brain networks in schizophrenia. J Neurosci 2010;30(28):9477-9487.

28. Rubinov M, Sporns O. Complex network measures of brain connectivity: Uses and interpretations. Neuroimage 2010;52(3):1059-1069.

29. Xu X, Hui ES, Mok MY, Jian J, Lau CS, Mak HK. Structural brain network reorganization in patients with neuropsychiatric systemic lupus erythematosus. AJNR Am J Neuroradiol 2017;38(1):64-70.

30. Hashimoto R, Hirata Y, Asada T, et al. Effect of the brain-derived neurotrophic factor and the apolipoprotein E polymorphisms on disease progression in preclinical Alzheimer's disease. Genes Brain Behav 2009;8 (1):43-52.

31. Heise V, Filippini N, Trachtenberg AJ, Suri S, Ebmeier KP, Mackay CE. Apolipoprotein E genotype, gender and age modulate connectivity of the hippocampus in healthy adults. Neuroimage 2014;98:23-30.

32. Chen Y, Liu Z, Zhang J, et al. Precuneus degeneration in nondemented elderly individuals with APOE varepsilon4: Evidence from structural and functional MRI analyses. Hum Brain Mapp 2017;38(1):271-282.

33. Lundstrom BN, Ingvar M, Petersson KM. The role of precuneus and left inferior frontal cortex during source memory episodic retrieval. Neuroimage 2005;27(4):824-834.

34. Miller EK, Li L, Desimone R. A neural mechanism for working and recognition memory in inferior temporal cortex. Science 1991;254(5036): 1377-1379.

35. Dik MG, Jonker C, Comijs HC, et al. Memory complaints and APOE-4 accelerate cognitive decline in cognitively normal elderly. Neurology 2001;57(12):2217-2222.

36. Zagha E, McCormick DA. Neural control of brain state. Curr Opin Neurobiol 2014;29:178-186.

37. Kohl MM, Shipton OA, Deacon RM, Rawlins JN, Deisseroth K, Paulsen O. Hemisphere-specific optogenetic stimulation reveals left-right asymmetry of hippocampal plasticity. Nat Neurosci 2011;14(11): 1413-1415.

38. Shinohara Y, Hirase H, Watanabe M, Itakura M, Takahashi M, Shigemoto R. Left-right asymmetry of the hippocampal synapses with differential subunit allocation of glutamate receptors. Proc Natl Acad Sci U S A 2008;105(49):19498-19503.

39. Han SD, Bondi MW. Revision of the apolipoprotein E compensatory mechanism recruitment hypothesis. Alzheimers Dement 2008;4(4): 251-254.

40. Ramadan S, Lin A, Stanwell P. Glutamate and glutamine: A review of in vivo MRS in the human brain. NMR Biomed 2013;26(12):1630-1646.